Quaternary Geochronology 29 (2015) 104–115

Contents lists available at ScienceDirect

Quaternary Geochronology

journal homepage: www.elsevier.com/locate/quageo

Research paper

A new Scandinavian reference ^{10}Be production rate

Arjen P. Stroeven [a, *], Jakob Heyman [a], Derek Fabel [b], Svante Björck [c], Marc W. Caffee [d, e], Ola Fredin [f], Jonathan M. Harbor [e]

[a] Geomorphology and Glaciology, Department of Physical Geography, and Bolin Centre for Climate Research, Stockholm University, S-106 91 Stockholm, Sweden
[b] School of Geographical and Earth Sciences, The University of Glasgow, Glasgow, UK
[c] Department of Geology, Quaternary Sciences, Lund University, Lund, Sweden
[d] Department of Physics and Astronomy/Purdue Rare Isotope Measurement Laboratory, Purdue University, West Lafayette, USA
[e] Department of Earth, Atmospheric, and Planetary Sciences, Purdue University, West Lafayette, USA
[f] Geological Survey of Norway, Trondheim, Norway

ARTICLE INFO

Article history:
Received 24 December 2014
Received in revised form
6 June 2015
Accepted 9 June 2015
Available online 12 June 2015

Keywords:
Cosmogenic exposure dating
^{10}Be production rate
Fennoscandian Ice Sheet
Deglaciation chronology
Baltic Ice Lake
Younger Dryas

ABSTRACT

An important constraint on the reliability of cosmogenic nuclide exposure dating is the rigorous determination of production rates. We present a new dataset for ^{10}Be production rate calibration from Mount Billingen, southern Sweden, the site of the final drainage of the Baltic Ice Lake, an event dated to 11,620 ± 100 cal yr BP. Five samples of flood-scoured bedrock surfaces (58.5°N, 13.7°E, 105–120 m a.s.l.) unambiguously connected to the drainage event yield a reference ^{10}Be production rate of 4.19 ± 0.20 atoms g^{-1} yr^{-1} for the CRONUS-Earth online calculator Lm scaling and 4.02 ± 0.18 atoms g^{-1} yr^{-1} for the nuclide specific LSD$_n$ scaling. We also recalibrate the reference ^{10}Be production rates for four sites in Norway and combine three of these with the Billingen results to derive a tightly clustered Scandinavian reference ^{10}Be production rate of 4.13 ± 0.11 atoms g^{-1} yr^{-1} for the CRONUS Lm scaling and 3.95 ± 0.10 atoms g^{-1} yr^{-1} for the LSD$_n$ scaling scheme.

1. Introduction

The cosmogenic nuclide exposure-age dating method is based on the accumulation of nuclides in minerals exposed to cosmic rays (Gosse and Phillips, 2001). All minerals contain the atomic targets for the production of cosmogenic nuclides, but only a few minerals are suitable for exposure age dating. Quartz (SiO_2), one of the most abundant minerals at the Earth's surface, retains the radionuclides ^{10}Be and ^{26}Al and the stable nuclide ^{21}Ne, their concentrations increasing with the time of exposure to cosmic rays. If the rate of nuclide production is known for a certain location on Earth an exposure duration can be calculated from the measured nuclide concentration.

Production rates of cosmogenic nuclides vary spatially and temporally. The production increases rapidly with altitude as a thinner atmosphere (at higher altitude) provides less interaction with the incoming cosmic rays. Cosmogenic nuclide production is lower towards the equator because the magnetic field more strongly deflects incoming cosmic rays at low latitudes (Nishiizumi et al., 1989; Gosse and Phillips, 2001). Temporal variations in cosmogenic nuclide production rates are caused by variations in the strength of the geomagnetic field (Nishiizumi et al., 1989; Masarik et al., 2001), solar activity (Lifton et al., 2005), and variations in atmospheric pressure (Staiger et al., 2007). Numerous investigations have considered issues that are relevant to models that scale production rates over varying geographic locations and time (Lal, 1991; Dunai, 2000, 2001; Stone, 2000; Desilets and Zreda, 2003; Lifton et al., 2005, 2008, 2014; Desilets et al., 2006; Argento et al., 2015 a, b).

Nuclide production rates have been of concern since the first applications of the technique in Earth Sciences (Klein et al., 1986; Kurz, 1986a, b; Nishiizumi et al., 1986, 1989; Phillips et al., 1986; Lal, 1991). Most of these initial studies focused on the mineral quartz because of its abundance in Earth's crust and on the ^{10}Be isotope because *in-situ* produced ^{10}Be can be separated from ^{10}Be produced in the atmosphere (Brown et al., 1991; Kohl and Nishiizumi, 1992).

To calculate an exposure age from a ^{10}Be concentration we

* Corresponding author.
E-mail address: arjen.stroeven@natgeo.su.se (A.P. Stroeven).

http://dx.doi.org/10.1016/j.quageo.2015.06.011
1871-1014/

calculate a site-specific ^{10}Be production rate by adopting a reference sea level high-latitude ^{10}Be production rate and a scaling method for calculating the geographic and temporal variations of ^{10}Be production. The reference ^{10}Be production rate is derived from ^{10}Be concentration measurements of samples having independent age control. If a scaling model incorporates all the relevant physics and temporal changes in production rate and it is coupled to an accurate reference production rate, it should reliably predict cosmogenic production rates at all locations. This approach was applied in the CRONUS-Earth calculator (Balco et al., 2008) with five production rate scaling schemes presented with associated average global reference ^{10}Be and ^{26}Al production rates. A number of subsequent site-specific production rate studies have, however, shown that the reference ^{10}Be production rates are ~5–15% lower than the original reference production rates (Balco et al., 2009; Putnam et al., 2010; Fenton et al., 2011; Kaplan et al., 2011; Ballantyne and Stone, 2012; Briner et al., 2012; Goehring et al., 2012b; Blard et al., 2013; Young et al., 2013; Claude et al., 2014; Kelly et al., 2015).

Here we report the first ^{10}Be production rate study from Sweden as a part of a larger study to assess the use of cosmogenic nuclides in ice sheet deglaciation reconstructions (e.g., Stroeven et al., 2011) and the production of a new deglaciation map of Fennoscandia (Stroeven et al., in review). We analyse 10 samples that are related to the final drainage of the Baltic Ice Lake in southern Sweden (Fig. 1) at the end of the Younger Dryas, and use a sub-sample of five bedrock samples to derive spallation reference ^{10}Be production rates using the CRONUS and the LSD production rate scaling schemes (Balco et al., 2008; Lifton et al., 2014). We further recalibrate the spallation reference ^{10}Be production rates from four sites in western Norway (Fenton et al., 2011; Goehring et al., 2012b, Fig. 1) and combine the Norway and Sweden data to derive a Scandinavian spallation reference ^{10}Be production rate for exposure dating and erosion rate studies.

2. Regional setting

2.1. Deglaciation history

The spatial pattern of shrinkage of the Fennoscandian Ice Sheet from its maximum position during the last glacial cycle has been mapped out using geomorphological traces (Kleman et al., 1997; Boulton et al., 2001; Stroeven et al., in review). This information has been augmented by a long history of geochronological studies, including G. De Geer's pioneering work on varve chronologies (De Geer, 1884, 1896, 1912, 1940). The formation of varves is intimately linked to the presence of freshwater basins that formed in association with changing ice sheet extents.

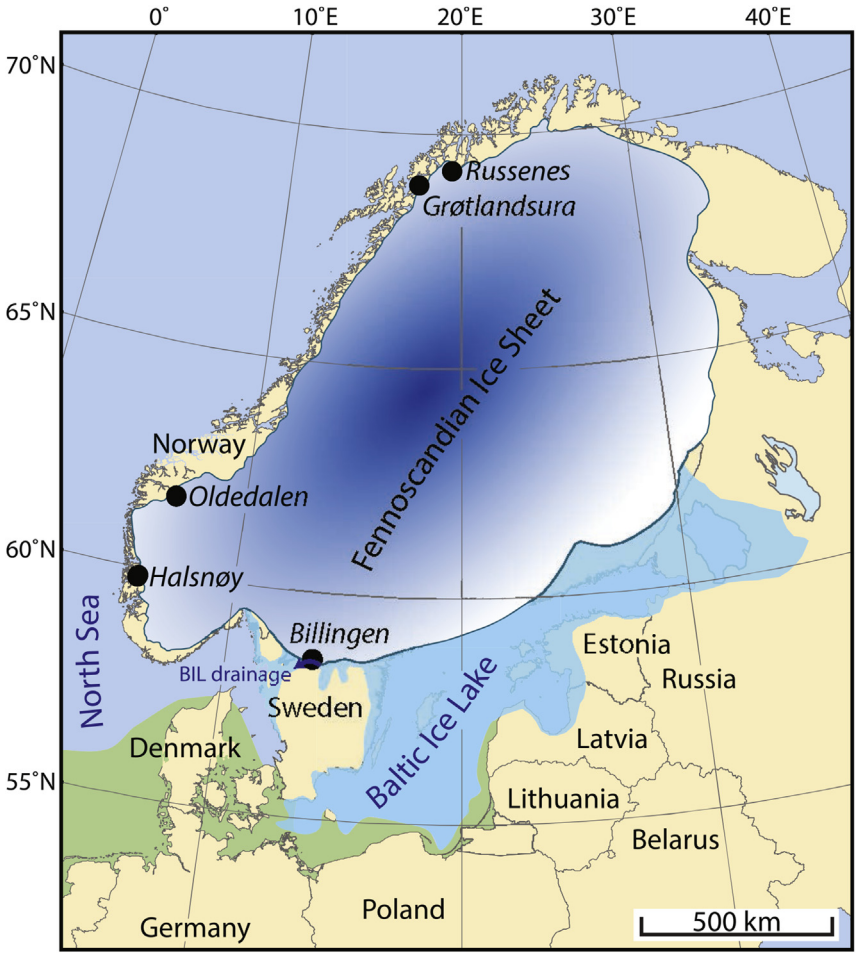

Fig. 1. Baltic Ice Lake and Fennoscandian Ice Sheet towards the end of the Younger Dryas (ice limit from Stroeven et al., in review). Prior to the catastrophic drainage of the Baltic Ice Lake at the northern tip of Mount Billingen (Fig. 2), the lake level was c. 25 m higher than contemporaneous sea level. Indicated are the four ^{10}Be calibration sites in Norway mentioned in the text. The extent of the Younger Dryas landbridge across Øresund, connecting Germany to Denmark–Sweden (green colour) after the final Baltic Ice Lake drainage, has been outlined after Andrén (2012). (For interpretation of the references to colour in this figure legend, the reader is referred to the web version of this article.)

The glacial Baltic Ice Lake (Fig. 1) was formed in the depression of the current Baltic Sea around 15.0–14.5 cal ka BP (Björck, 1995). Its development and history was conditioned by isostatic uplift of its outlet in Øresund (Fig. 1). When the ice sheet margin retreated northwards during the Bølling and Allerød warm phases, the Øresund outlet rose above sea level around 14.0 cal ka BP because isostatic rebound was more rapid than eustatic sea level rise. The Baltic Ice Lake was extant until the end of the Younger Dryas, although it probably experienced a smaller (5–10 m) drainage event at the end of the Allerød period, dated to c. 13.0 cal ka BP (Björck, 2008), following significant ice margin retreat. An ice readvance during the Younger Dryas (Björck and Digerfeldt, 1984) re-established the ice dam and allowed the Baltic Ice Lake to fill to higher levels again. When the ice sheet margin retracted from its position at the end of the Younger Dryas a drainage channel opened up at the northern tip of Mount Billingen (Fig. 1), a table-mountain bedrock ridge, allowing the Baltic Ice Lake to drain catastrophically into the North Sea west of Mount Billingen with a contemporaneous sea level at the present-day elevation of 125 m above sea level [a.s.l.], which was c. 25 m below the level of the Baltic Ice Lake.

The cessation of the Younger Dryas is an important phase in ice sheet and environmental reconstructions in the Baltic region. When the ice dam at Mount Billingen failed, the Baltic Ice Lake drained to a much lower level, with severe impacts on downstream landscapes through erosion and deposition, lowered regional salinity levels as freshwater mixed into the ocean, and elevated salinity of the Baltic within a few hundred years after the drainage at the start of the Yoldia Sea stage. The significance of this drainage event in Scandinavian glacial history is best reflected by the fact that it has attracted over 100 years of research (Munthe, 1910, 1912, 1928, 1940; Lundqvist, 1921, 1931; Gavelin, 1926; Johansson, 1926, 1937; Westergård, 1926; Munthe et al., 1928; Sauramo, 1934, 1937, 1958; Bergsten, 1943; Caldenius, 1944; Cleve-Euler, 1946; Donner, 1969, 1978; Strömberg, 1974, 1977a, b, 1985, 1994; Björck, 1979, 1981, 1995; Mörner, 1979; Björck and Digerfeldt, 1984, 1986, 1989; Svensson, 1991; Björck et al., 1995; Bodén et al., 1997; Andrén et al., 1999, 2002; Lundqvist and Wohlfarth, 2001; Tikkanen and Oksanen, 2002; Jakobsson et al., 2007; Johnson et al., 2010).

2.2. Baltic Ice Lake

The drainage of the Baltic Ice Lake across the Mount Billingen threshold towards the North Sea and the North Atlantic at the very end of the Younger Dryas cold period is arguably the most dramatic event of the last deglaciation. The southern Fennoscandian Ice Sheet margin damming the 349,400 km^2 lake (Jakobsson et al., 2007) was located against the northern tip of Mount Billingen, a relatively low N–S water divide constraining the ice lake towards the west (Fig. 2). The characteristics of the Baltic Ice Lake as the ice sheet retreated from the northern tip of Mount Billingen have been analysed in a number of publications (Johansson, 1926; Olausson, 1982; Lambeck, 1999; Lindeberg, 2002) and most recently by Jakobsson et al. (2007) who also took into account differential bedrock rebound. According to their study the lake had a volume of 29,300 km^3 and stood at 151 m a.s.l. before the final drainage event. During a rapid release of 7800 km^3 of meltwater at the northern tip of Mount Billingen (at St. Stolan; Fig. 2), the Baltic Ice Lake area shrank by 18% (Lindeberg, 2002; Jakobsson et al., 2007) and the water level dropped to 125 m a.s.l., the local sea level elevation at the time (Strömberg, 1977a, b).

Strömberg (1992) identified flood deposits derived from Mount Billingen and suggested that the final drainage lasted several decades. Most authors, however, now consider the event to have progressed catastrophically with an estimated discharge of 0.12–0.30 Sv (1 Sv = 1×10^6 m^3 s^{-1}) over the duration of 1–2 years (Björck et al., 1996; Andrén et al., 2002; Lindeberg, 2002; Jakobsson et al., 2007; Johnson et al., 2013b). The evidence of the catastrophic drainage, apart from the bedrock sill at St. Stolan (which has now been almost completely removed by mining) comes from (i)

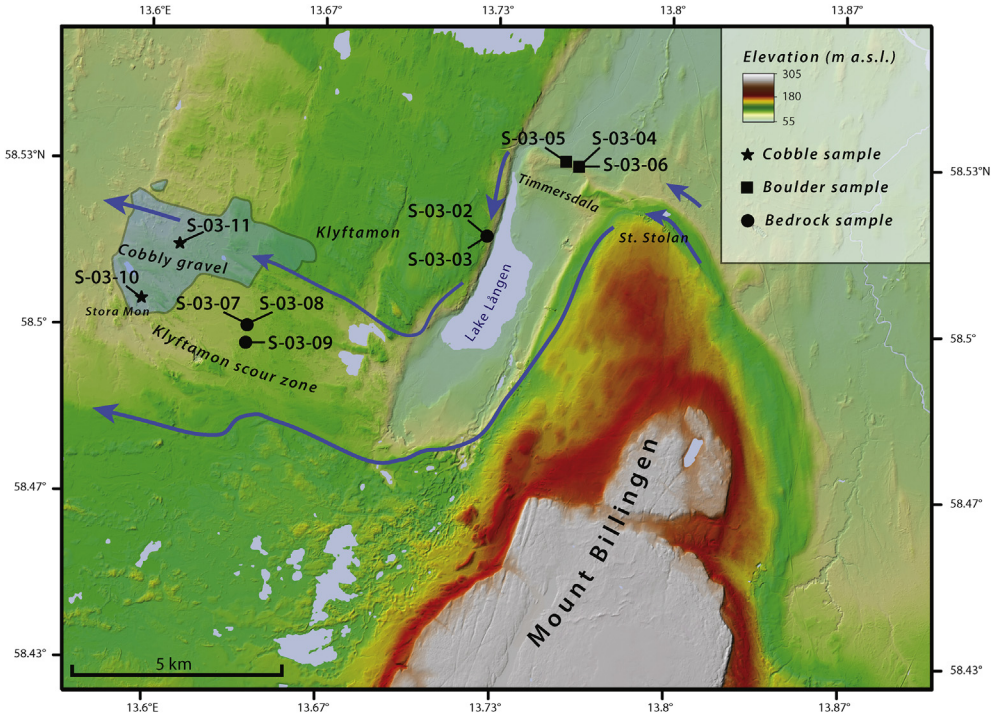

Fig. 2. Topographic map of the study region. Topographic map of the Mount Billingen area based on a LiDAR DEM with sample locations and the width of the Baltic Ice Lake catastrophic drainage path marked with blue arrows. (For interpretation of the references to colour in this figure legend, the reader is referred to the web version of this article.)

Klyftamon, a c. 20 km^2 area where all loose overburden has been removed and the bedrock shows P-forms (Figs. 2 and 3), (ii) very course boulder deposits just down-current from the Klyftamon area (Lundqvist, 1931; Björck and Digerfeldt, 1984), now being mined and available for inspection at Stora Mon, for example (Fig. 2), and deposited in c. 20–30 m of water depth, (iii) a fairly detailed description of the deposits connected to the drainage (Johnson et al., 2010), and (iv) meltwater $\delta^{18}O$ spikes in sedimentary sequences in Skagerrak, offshore of southwestern Sweden (Olausson, 1982; Erlenkeuser, 1985) and in onshore uplifted marine sequences (Bodén et al., 1997).

Following the Baltic Ice Lake drainage, all our sample locations were submerged under water. Based on relative sea level studies in southern Sweden (Svedhage, 1985; Björck and Digerfeldt, 1986; Påsse, 1987; Svensson, 1989) the emergence rate is estimated to have started at 4 cm yr^{-1} at the time of the drainage and to have averaged c. 3 cm yr^{-1} for the first 1000 years after the drainage.

2.3. Study region northwest of Mount Billingen

The study area is located in the middle Swedish end moraine zone which is rich in morphological traces of the glacial history of the region such as eskers, meltwater channels, perched deltas, highest shorelines, kame terraces, and end moraines/glaciofluvial complexes. Two major ice standstills are recognised and delineate the middle Swedish end moraine zone (Mörner, 1969; Berglund, 1976). The precise history of these moraines (Johnson et al., 2013a) and correlation of ice-marginal features west and east of Mount Billingen are still highly conjectural. This is mainly because, in contrast to the evidence west of Mount Billingen for ice-marginal oscillations, varves east of Mount Billingen indicate a steady retreat of the ice margin though at variable rates (Strömberg, 1994).

The region of interest for our production rate calibration study is located north of the end moraine zone and west of the northernmost protrusion of Mount Billingen, where the Baltic Ice Lake drainage occurred as the ice margin retreated (Figs. 1 and 2). West of the northern part of Mount Billingen, a 1.7–2.5 km wide basin including Lake Lången, at an altitude of 65 m a.s.l., separates Mount Billingen from Klyftamon, another low bedrock hill (at 130–140 m a.s.l.). Just north of the end moraine zone, the Klyftamon hill is cut by a c. 3 km wide and 20 m deep scour (Fig. 2). Large parts of this scour, in particular in the east, are characterized by bare bedrock with P-forms (Fig. 3), while there are sedimentary boulder and gravel deposits in the west (Johnson et al., 2010, 2013b). The Klyftamon scour and the boulder and gravel deposits are interpreted as erosional and depositional traces, respectively, from the Baltic Ice Lake drainage event (Strömberg, 1992; Johnson et al., 2010, 2013a, b). A large c. 2 km-long and 10–40 m high ridge – the Timmersdala ridge (Fig. 2) – extends in a WNW-ESE orientation from north of Lake Lången to west of the northern tip of Mount Billingen. This ridge has been interpreted as being formed by drainage deposits at the time of the Baltic Ice Lake drainage (Johansson, 1926, 1937; Johnson et al., 2010; Pizarro Rajala, 2012).

2.4. Independent age of the Baltic Ice Lake drainage

The timing of the final Baltic Ice Lake drainage has been discussed by many of the authors cited above (Hyttinen et al., 2014). The event clearly occurred when the ice sheet finally deglaciated from the northern tip of Mount Billingen, but direct age constraints for ice margin changes did not tightly constrain the drainage event. Studies accordingly focused on dating other indicators of the drainage event. Pollen stratigraphy, for example, and ^{14}C dating of shore displacement within the Baltic Ice Lake by Björck (1979) and Svensson (1989) showed that the Baltic Ice Lake level was lowered 25 m just before the so-called Younger Dryas–Preboreal transition zone (Berglund, 1966). The onset of this zone was correlated to the very onset of the Holocene in the GRIP ice core (Björck et al., 1996), and dated to 11,525 ice yr BP. Correlations between the varve record in the Baltic Ice Lake and the ^{18}O record from GRIP (Andrén et al., 2002) show that the drainage event, clearly seen in the varves, occurred 35 years before the onset of the Holocene. Refinement of the NGRIP ice core record shows that the Holocene starts at 11,700 ± 99 cal years b2k (Walker et al., 2009; Rasmussen et al., 2014), or 11,650 cal yr BP (AD 1950), but detailed statistical comparisons between ^{14}C in tree rings and ^{10}Be in ice cores (Muscheler et al., 2008) imply that the ice core record is 65 years too old. The best age of the start of the Holocene is therefore 11,585 cal yr BP and the drainage, being 35 years older, is dated to 11,620 cal yr BP (AD 1950), or 11,673 years before the sampling in 2003. We assign an uncertainty of 100 years to this drainage age as a combined uncertainty for the ice core record and the clay varve – ice core correlation.

The age of this catastrophic event is now sufficiently well constrained by multiple techniques to be used as a calibration site for cosmogenic nuclides. The event created severely scoured bedrock surfaces and transported large and small boulders now found in constructional morphologies and in flood deposits. Samples from such surfaces could help to independently constrain the production rate of cosmogenic isotopes. In this study we analyse ten samples

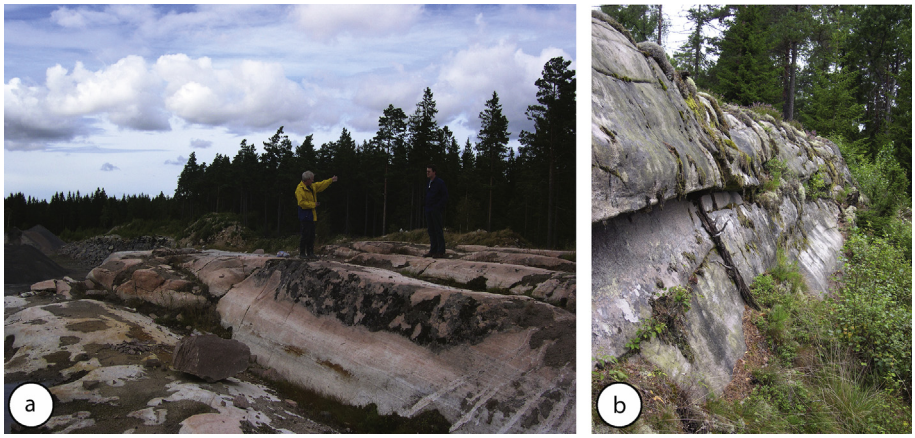

Fig. 3. Flood-scoured and streamlined bedrock surfaces at Klyftamon with P-forms. Occurrences of flood-scoured and streamlined bedrock surfaces in a) a gravel pit (where no samples were collected) and b) in the area where samples S-03-07 through S-03-09 were collected. The sample locations are detailed in Fig. 2.

Table 1
Baltic Ice Lake drainage sample data, including ^{10}Be concentrations. All uncertainties are at the 1 σ level.

Sample	Sample type	Lat (DD)	Long (DD)	Elevation (m a.s.l.)	Thickn. (cm)	Topo shielding	^{10}Be conc (atoms g^{-1})[a]	^{10}Be standard[b]	^{10}Be conc (atoms g^{-1}) 07KNSTD[c]
S-03-02	Bedrock	58.51890	13.72940	115	2	1	59,741 ± 3444	KNSTD	54,018 ± 3114
S-03-03	Bedrock	58.51890	13.72940	119	4	1	61,935 ± 2940	KNSTD	56,001 ± 2659
S-03-04	Boulder	58.53402	13.75966	95	2	1	57,339 ± 3679	KNSTD	51,846 ± 3327
S-03-05	Boulder	58.53402	13.75966	95	2	1	50,448 ± 3961	KNSTD	45615 ± 3582
S-03-06	Boulder	58.53320	13.76458	100	2	1	53,962 ± 5086	KNSTD	48,792 ± 4599
S-03-07	Bedrock	58.50032	13.63830	106	5	0.9954	57,758 ± 2240	KNSTD	52,225 ± 2026
S-03-08	Bedrock	58.50032	13.63830	105	5	0.9954	60,860 ± 2596	KNSTD	55,029 ± 2347
S-03-09	Bedrock	58.49664	13.63800	120	5	1	59,133 ± 4350	KNSTD	53,468 ± 3933
S-03-10	Cobbles	58.50514	13.59663	110	5	1	56,553 ± 2407	KNSTD	51,135 ± 2176
S-03-11	Cobble	58.51637	13.61215	105	10	1	43,495 ± 3124	NIST_30000	40,507 ± 2909

[a] The ^{10}Be concentrations are corrected for the measured number of ^{10}Be atoms in blanks, which represents <5% of the total ^{10}Be atoms of the samples.
[b] Samples S-03-02 to 10 were measured at PRIME Lab and standardized against the pre-Nishiizumi et al. (2007) standard, KNSTD. Sample S-03-11 was measured at SUERC and standardized against the NIST standard with an assumed ^{10}Be/^{9}Be isotope ratio of 3.0×10^{-11} (NIST_30000).
[c] Concentrations used for the production rate calibration. The ^{10}Be concentrations of the KNSTD and NIST_30000 samples were multiplied by 0.9042 and 0.9313, respectively, for conversion to the Nishiizumi et al. (2007) 07KNSTD standardization.

for their concentrations of ^{10}Be in quartz.

3. Materials and methods

3.1. Billingen sampling and ^{10}Be measurements

We collected ten samples from four sites in 2003 (Fig. 2; Table 1). We sampled quartz veins in gneiss from the tops of flood-scoured bedrock surfaces, and quartz-rich boulders and cobbles from depositional landforms along the postulated floodway of the last Baltic Ice Lake drainage to the west of northern Mount Billingen (Figs. 2 and 4). Three samples were collected from the tops of large (>2 × 2 × 2 m) sandstone boulders on the Timmersdala ridge (S-03-04,-05,-06). Two samples were collected from bedrock (S-03-02,-03) west of Lake Lången, near the top of a very steep, fault-controlled slope that separates the Lake Lången basin from Klyftamon. Three samples were collected from meltwater-scoured bedrock surfaces (S-03-07,-08,-09) in the Klyftamon scour. Finally, two samples were collected from the drainage deposits further west with one sample consisting of three amalgamated cobbles (S-03-10; c. 5 cm) near the Stora Mon gravel quarry and a single cobble sample (S-03-11; c. 10 cm) near a gravel quarry 1.2 km NNE of the latter site. All the sample locations, at 95–120 m a.s.l., were initially located 5–30 m below sea level. Hence, for some part of their post-drainage exposure history they had to travel through the shallow sea water column.

Quartz separation and purification was carried out using methods modified from Kohl and Nishiizumi (1992) and Child et al. (2000). Beryllium isotope ratios were measured by AMS at PRIME Lab (samples S-03-02 to 10) with standardization against the pre-Nishiizumi et al. (2007) ICN ^{10}Be standard (CRONUS calculator KNSTD) and at SUERC (sample S-03-11) with standardization against the NIST ^{10}Be standard with an assumed ^{10}Be/^{9}Be isotope ratio of 3.0×10^{-11} (CRONUS calculator NIST_30000). To normalize the ^{10}Be concentrations to the updated 07KNSTD standardization of Nishiizumi et al. (2007), the KNSTD and NIST_30000 samples were multiplied by 0.9042 and 0.9313, respectively (Table 1).

3.2. Billingen production rate calibration

To determine ^{10}Be production rates based on the Mount Billingen samples we adjusted the reference ^{10}Be production rate to derive the best fit (reduced chi-square χ^2_R minimization) between calculated exposure ages for each sample and the calibration age of 11,673 years before sampling. The ^{10}Be concentrations were re-standardized to the Nishiizumi et al. (2007) ICN ^{10}Be standard (CRONUS calculator 07KNSTD) against which the calculated ^{10}Be production rates are referenced. We used a modified version of the

Fig. 4. Illustration of sampling environments. a) Sampling location along Lake Lången on a coarse-grained gneiss bedrock rib (Sample S-03-03) interpreted to be cut by catastrophic drainage of the Baltic Ice Lake. b) Sampling a large sandstone boulder (S-03-04) on the Timmersdala ridge immediately west of the northern tip of Mount Billingen. c) Sampling of a thick quartz vein at Klyftamon (S-03-07), another fluvially-washed bedrock surface.

CRONUS calculator code (version 2.2, constants file 2.2.1) for the exposure age calculations adopting the CRONUS scaling schemes St, De, Du, Li, and Lm (Balco et al., 2008) with the internal (analytical) exposure age uncertainty used for χ^2_R calculations. We use a density of 2.65 g cm^{-3} for rock shielding corrections and we assume zero post-depositional erosion and shielding by snow for all samples; we did not observe any evidence of erosion. The ^{10}Be decay constant is defined by its half-life of 1.387 Ma (Chmeleff et al., 2010; Korschinek et al., 2010). The time-constant CRONUS calculator ^{10}Be production due to muons is included in the exposure age calculation to derive the reference production rate for ^{10}Be by spallation.

To determine the spallation reference ^{10}Be production rates for LSD scaling schemes (general spallation LSD_g and ^{10}Be nuclide-specific LSD_n) we used the same code as for the CRONUS production rate calibration except that the muogenic production rate and spallogenic production rate scaling schemes were derived from Lifton et al. (2014). We adjusted the reference ^{10}Be production rate with χ^2_R minimization to match the exposure ages to the calibration age of 11,673 years before sampling. The LSD production rate scaling is based on a modelling of the atmospheric cosmic ray particle flux (Sato et al., 2008). This contrasts with the CRONUS production rate scaling schemes which are based on photo-emulsions and/or neutron monitor data (Balco et al., 2008). The LSD scaling schemes of Lifton et al. (2014) further use an atmospheric pressure interpolation based on ERA-40 (which yields <0.02% difference from the CRONUS calculator NCEP atmospheric pressure for all production rate samples included in this study) and a new temporal scaling for geomagnetic and solar variations that is used for both the spallogenic and muogenic production pathways (constant for the CRONUS scaling schemes). The temporal scaling of the LSD production rates has been adjusted to the year of sampling (2003). Note that this adjustment was only applied to the LSD scaling schemes and not the CRONUS scaling schemes in order to keep the production rate calibration in line with the online exposure age calculator. Sample thickness-, topographic shielding-, and erosion corrections, and the calculation of exposure ages and analytical uncertainties are the same in the LSD production rate calibration as in the CRONUS calculator.

Because all sampled surfaces were located under water after the drainage event, the ^{10}Be production while submerged has been corrected with a water density of 1.02 g cm^{-3} and the submergence duration, which is a function of the thickness of the water column and local emergence rates. We use an exponential function to define the emergence rate v (cm yr^{-1}) as a function of duration after the Baltic Ice Lake drainage t (yr):

$$v = 4.0\, e^{-0.0005\, t} \quad (1)$$

where 4.0 represents the initial emergence rate (cm yr^{-1}). This yields submergence durations ranging from 129 to 940 years for the ten samples (Fig. 5). The spallogenic production is corrected for an exponential decrease using the CRONUS spallation attenuation length of 160 g cm^{-2} and the muogenic production is calculated based on Balco et al. (2008; P_mu_total) for the CRONUS scaling schemes and Lifton et al. (2014; P_mu_totalLSD) for the LSD scaling schemes. After exhumation through the water column, we assume a constant elevation defined by the present-day elevation of the samples. This assumption will yield a lower production rate compared to a model including isostatic uplift (Goehring et al., 2012a) but it is motivated by the fact that exposure age calculations typically disregard the effects of isostatic uplift (Young et al., 2013). We use an iteration process to arrive at the production rate which, given the sample emergence history, yields the measured ^{10}Be concentration in the sample. For all scaling schemes the calibration age uncertainty of 100 years is added in quadrature using

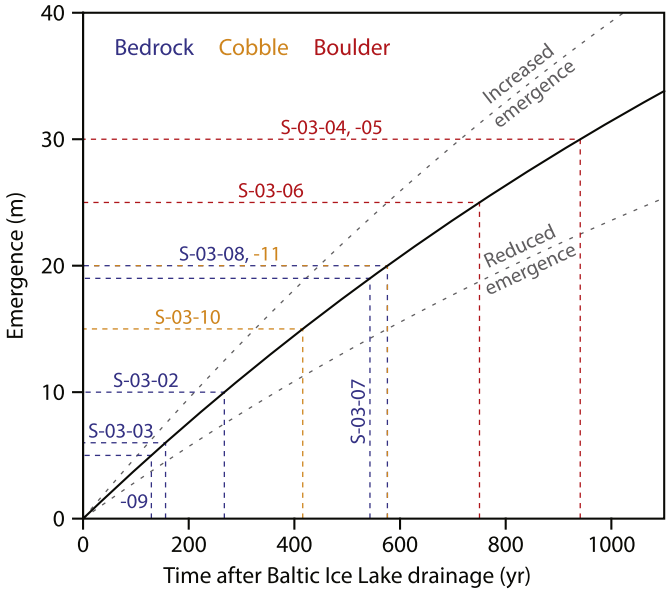

Fig. 5. Shore displacement curve for the Mount Billingen area (Svedhage, 1985; Björck and Digerfeldt, 1986; Påsse, 1987; Svensson, 1989). The ten samples that compose the Mount Billingen ^{10}Be production rate are plotted on the curve so that depth below sea level immediately after the catastrophic drainage of the Baltic Ice Lake (y-axis) determines the timing of emergence on the x-axis. Increased and reduced emergence rates used for testing the sensitivity of the production rate calibration to the initial emergence rate uncertainty are illustrated by the dashed curves.

standard error propagation. We also performed a sensitivity test of the emergence rate uncertainty for the ^{10}Be production rate calibration using Equation (1) with increased (5.0 cm yr^{-1}) and reduced (3.0 cm yr^{-1}) initial emergence rates (Fig. 5). These emergence rates bracket the uncertainty span in the local emergence rate, with the increased emergence rate yielding 39 m of emergence and the reduced emergence rate yielding 24 m of emergence within the first 1000 years following the Baltic Ice Lake drainage.

3.3. Recalibration of Norway ^{10}Be production rates

To obtain Scandinavian ^{10}Be production rates we have recalibrated the CRONUS and LSD ^{10}Be production rates for two sites in northern Norway (Fenton et al., 2011) and two sites in southwestern Norway (Goehring et al., 2012b). The recalibration was carried out similar to the Mount Billingen site but without exhumation through water. The input data is derived from the original publications with a few minor changes (see the Supplementary material). The radiocarbon calibration ages for all four sites are recalibrated to the IntCal13 curve (Reimer et al., 2013) using OxCal 4.2 (Bronk Ramsey, 2009) and adjusted to the sampling year (Heyman, 2014).

The two northern Norway calibration sites are the Grøtlandsura and Russenes rock avalanches (Fenton et al., 2011). Both rock avalanches occurred shortly after deglaciation and from each of the two sites ^{10}Be has been measured in three boulder samples. The calibration age of the Grøtlandsura rock avalanche is based on two radiocarbon dates from marine shells (corrected for a marine reservoir effect of 440 years) which, after recalibration against the IntCal13 curve, yield a calibration age of 11,438 ± 118 years before sampling. The calibration age of the Russenes rock avalanche is based on three radiocarbon dates from marine shells (corrected for a marine reservoir effect of 440 years) which, after recalibration against the IntCal13 curve, yield a calibration age of 10,996 ± 111

years before sampling. We adopt the Fenton et al. (2011) adjustments for moss- and snow shielding for the northern Norway sites and express this shielding in "cm of rock shielding" (using a density of 2.65 g cm^{-3}). This way, the moss- and snow shielding is also taken into account for the muogenic production pathway. Similar to Fenton et al. (2011), we assume zero post-depositional erosion for all calibration samples from northern Norway.

The two western Norway sites are the Younger Dryas Halsnøy moraine and the Oldedalen rock avalanche (Goehring et al., 2012b). The Halsnøy moraine and Oldedalen rock avalanche sites include ^{10}Be data from eight moraine boulder samples and six rock avalanche block samples, respectively. The calibration age of the Halsnøy moraine is based on the radiocarbon dated Eplandmyr stratigraphy presented in Lohne et al. (2012: Supplementary OxCal code) which, recalibrated against the IntCal13 curve, yields a calibration age of 11,648 ± 110 years before sampling. The calibration age of the Oldedalen rock avalanche is based on a single radiocarbon age from outer wood of a tree overrun by the rock avalanche, yielding a calibration age of 6067 ± 111 years before sampling. Similar to Goehring et al. (2012b), we assume an erosion rate of 0.172 cm ka^{-1} for the Halsnøy moraine samples and zero post-depositional erosion for the Oldedalen rock avalanche samples. For both sites we assume no shielding by snow. In the original production rate calibration (Goehring et al., 2012b) a correction for isostatic uplift was included for the Halsnøy moraine site. Similar to Young et al. (2013), we have chosen not to include this uplift correction because uplift corrections are typically not included when using reference production rates to calculate exposure ages.

3.4. Calibration strategy

For each calibration site, we first calibrate the ^{10}Be production rates based on the full dataset, except for the Halsnøy moraine site for which we exclude the two samples identified as outliers by Goehring et al. (2012b). To derive production rates based only on tightly clustered ^{10}Be data, we demand the datasets to satisfy $\chi^2_R < 1.5$ and we therefore seek the maximum number of samples at each site that satisfies this criterion. Requiring that $\chi^2_R < 1.5$ for each dataset ensures that the data will be tightly clustered, reducing the risk of inclusion of samples with prior and/or incomplete exposure. For calibration sites where $\chi^2_R > 1.5$, we thus derive two reference ^{10}Be production rates for each scaling scheme; group A, based on the full dataset, hence more inclusive, with the original (larger) scatter and a group B with a restricted selection of samples requiring a well-clustered production rate. For the Mount Billingen calibration site, we further calibrate the production rates for bedrock samples (N = 5), boulder samples (N = 3), and boulder and cobble samples (N = 5), in order to evaluate the potential differences between the sample types.

4. Results

The Mount Billingen data for the Baltic Ice Lake drainage event is presented in Table 1 and ^{10}Be production rates are presented in Table 2. In the following text, we present the reference production rates for the LSD_n scaling scheme. For information on the production rates of the other six scaling schemes we refer to the tables and the Supplementary material. The individual samples yield LSD_n reference production rates ranging from 3.19 ± 0.23 to 4.22 ± 0.18 atoms g^{-1} yr^{-1} (Table 2; Fig. 6). The LSD_n reference production rate based on all ten samples is 3.88 ± 0.21 atoms g^{-1} yr^{-1} ($\chi^2_R = 1.56$) (Table 2) and the data is somewhat skewed with a tail towards lower production rates (Fig. 6). If sample S-03-11 with the lowest ^{10}Be concentration is excluded, the remaining nine samples yield a better clustered reference production rate of 3.94 ± 0.21 atoms g^{-1} yr^{-1} ($\chi^2_R = 0.68$). The five bedrock samples yield well-clustered production rates in the higher part of the range (LSD_n 4.02 ± 0.18 atoms g^{-1} yr^{-1}; $\chi^2_R = 0.45$), the three boulder samples yield slightly lower well-clustered production rates (LSD_n 3.77 ± 0.26 atoms g^{-1} yr^{-1}; $\chi^2_R = 0.74$), and the five boulder and cobble samples yield more scattered production rates (LSD_n 3.67 ± 0.23 atoms g^{-1} yr^{-1}; $\chi^2_R = 1.63$). The sample emergence through the water column reduces the ^{10}Be production rate for the first 129–940 years, resulting in 0.8–8.1% higher individual sample production rates when included. Adopting increased and reduced emergence rates only yield <1.1% difference in the reference production rates for the full set of samples, <1.1% difference in the reference production rates for the bedrock samples, and <3.8% difference in the reference production rates for the boulder samples. These uncertainties are significantly lower than the uncertainty introduced by measurement uncertainties, indicating that the production rate calibration is relatively insensitive to initial emergence rate variations (Fig. 5).

The site-specific production rates for the four Norwegian

Table 2
Individual sample and combined (based on chi square minimization) Baltic Ice Lake drainage spallation reference ^{10}Be production rates for the five CRONUS scaling schemes (Balco et al., 2008) and the two LSD scaling schemes (Lifton et al., 2014). All uncertainties are at the 1 σ level.

Sample	St (at g^{-1} yr^{-1})	De (at g^{-1} yr^{-1})	Du (at g^{-1} yr^{-1})	Li (at g^{-1} yr^{-1})	Lm (at g^{-1} yr^{-1})	LSD_g (at g^{-1} yr^{-1})	LSD_n (at g^{-1} yr^{-1})
S-03-02	4.04 ± 0.24	4.15 ± 0.24	4.16 ± 0.24	4.43 ± 0.26	4.04 ± 0.24	3.89 ± 0.23	3.88 ± 0.23
S-03-03	4.20 ± 0.20	4.32 ± 0.21	4.33 ± 0.21	4.62 ± 0.22	4.20 ± 0.20	4.05 ± 0.20	4.04 ± 0.20
S-03-04	4.20 ± 0.27	4.31 ± 0.28	4.31 ± 0.28	4.60 ± 0.30	4.20 ± 0.27	4.03 ± 0.26	4.02 ± 0.26
S-03-05	3.67 ± 0.29	3.77 ± 0.30	3.77 ± 0.30	4.03 ± 0.32	3.67 ± 0.29	3.53 ± 0.28	3.52 ± 0.28
S-03-06	3.85 ± 0.37	3.95 ± 0.38	3.96 ± 0.38	4.23 ± 0.40	3.85 ± 0.37	3.71 ± 0.35	3.69 ± 0.35
S-03-07	4.15 ± 0.17	4.26 ± 0.17	4.27 ± 0.17	4.56 ± 0.18	4.15 ± 0.17	4.00 ± 0.16	3.98 ± 0.16
S-03-08	4.40 ± 0.19	4.52 ± 0.20	4.53 ± 0.20	4.83 ± 0.21	4.40 ± 0.19	4.23 ± 0.19	4.22 ± 0.18
S-03-09	4.02 ± 0.30	4.14 ± 0.31	4.15 ± 0.31	4.42 ± 0.33	4.03 ± 0.30	3.88 ± 0.29	3.87 ± 0.29
S-03-10	3.98 ± 0.17	4.09 ± 0.18	4.10 ± 0.18	4.37 ± 0.19	3.98 ± 0.17	3.83 ± 0.17	3.82 ± 0.17
S-03-11	3.31 ± 0.24	3.40 ± 0.25	3.41 ± 0.25	3.63 ± 0.26	3.31 ± 0.24	3.20 ± 0.23	3.19 ± 0.23
Combined (N = 10)	**4.04 ± 0.23**	**4.15 ± 0.24**	**4.16 ± 0.24**	**4.44 ± 0.25**	**4.04 ± 0.23**	**3.89 ± 0.21**	**3.88 ± 0.21**
X^2_R	1.51	1.52	1.51	1.54	1.51	1.56	1.56
Combined (N = 9)	**4.11 ± 0.23**	**4.22 ± 0.23**	**4.23 ± 0.23**	**4.51 ± 0.25**	**4.11 ± 0.23**	**3.95 ± 0.21**	**3.94 ± 0.21**
X^2_R	0.66	0.66	0.66	0.66	0.65	0.68	0.68
Bedrock (N = 5)	**4.19 ± 0.20**	**4.31 ± 0.20**	**4.31 ± 0.20**	**4.60 ± 0.22**	**4.19 ± 0.20**	**4.04 ± 0.18**	**4.02 ± 0.18**
X^2_R	0.45	0.44	0.44	0.44	0.45	0.44	0.45
Boulder (N = 3)	**3.93 ± 0.28**	**4.03 ± 0.28**	**4.04 ± 0.29**	**4.31 ± 0.30**	**3.93 ± 0.28**	**3.78 ± 0.26**	**3.77 ± 0.26**
X^2_R	0.72	0.72	0.72	0.74	0.72	0.74	0.74
Boulder/cobble (N = 5)	**3.83 ± 0.24**	**3.93 ± 0.25**	**3.94 ± 0.25**	**4.20 ± 0.26**	**3.83 ± 0.24**	**3.68 ± 0.23**	**3.67 ± 0.23**
X^2_R	1.57	1.57	1.56	1.59	1.57	1.63	1.63

calibration sites (Fig. 1) are presented in Table 3 (see the Supplementary material for individual sample reference ^{10}Be production rates). The Grøtlandsura and Russenes sites in northern Norway both yield well-clustered LSD_n production rates of 3.45 ± 0.14 atoms g^{-1} yr^{-1} (χ^2_R = 0.79) and 3.82 ± 0.19 atoms g^{-1} yr^{-1} (χ^2_R = 0.82), respectively. The Halsnøy moraine site yields an LSD_n production rate of 4.05 ± 0.10 atoms g^{-1} yr^{-1} (χ^2_R = 3.11) for the full set of samples and after rejection of two samples to fulfil the χ^2_R < 1.5 criterion, the remaining six samples yield an LSD_n production rate of 4.04 ± 0.11 atoms g^{-1} yr^{-1} (χ^2_R = 1.29). The Oldedalen rock avalanche site yields an LSD_n production rate of 3.99 ± 0.13 atoms g^{-1} yr^{-1} (χ^2_R = 2.00) with two samples rejected as outliers (Goehring et al., 2012b), and 3.90 ± 0.13 atoms g^{-1} yr^{-1} (χ^2_R = 0.59) with three samples rejected as outliers to fulfil the χ^2_R < 1.5 criterion.

5. Discussion

The production rates for the ten Mount Billingen samples are skewed with a tail towards low production rates indicating that incomplete exposure may have resulted in exceedingly low ^{10}Be concentrations in some samples (Blard et al., 2007; Applegate et al., 2010; Heyman et al., 2011). The five bedrock samples yield a well-clustered production rate (4.02 ± 0.18 atoms g^{-1} yr^{-1}) that is slightly higher, but within statistical uncertainties, than a similarly well-clustered production rate for the three boulder samples (3.77 ± 0.26 atoms g^{-1} yr^{-1}; Table 2). There are two possible ways to explain why bedrock surfaces yield slightly higher production rates than boulder samples. First, the bedrock surfaces may have experienced insufficient erosion and therefore retain an inheritance signal due to prior exposure. Second, the boulder (and cobble) samples may have experienced incomplete exposure due to post-glacial shielding, typical for degrading landforms (cf. Putkonen et al., 2008). The five bedrock samples are derived from three separate locations along the Baltic Ice Lake drainage corridor (Fig. 2) and it appears highly unlikely that each of these three locations would have experienced just the same amount of limited erosion necessary to result in a similar amount of inheritance in all five samples. Further, the overall topography of the area from where the bedrock surfaces have been collected, with a clear erosional depression due to fluvial erosion across the scoured region of Klyftamon, supports an interpretation with more than just a few metres of erosion. The lowest individual sample production rate comes from cobble sample S-03-11. Conceptual landform

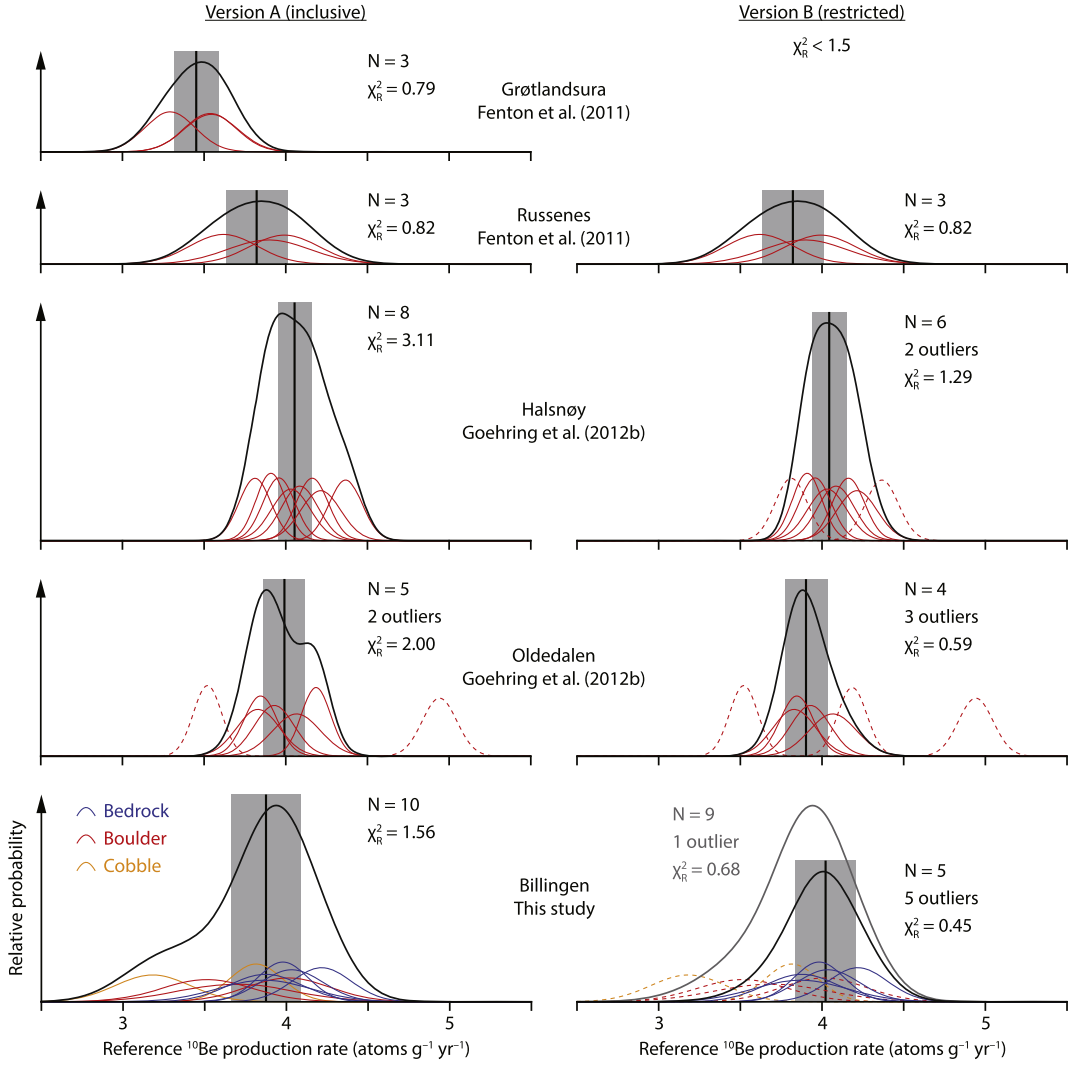

Fig. 6. Individual sample and location reference ^{10}Be production rates as probability density distributions using the LSD_n scaling scheme for five locations in Scandinavia. The probability density distributions in this figure are based on the production rate uncertainty before including the calibration age uncertainty as the uncertainty of the calibration age is not independent for the individual samples of each site.

Table 3
Scandinavian site-specific and average spallation reference ^{10}Be production rates for the five CRONUS scaling schemes (Balco et al., 2008) and the two LSD scaling schemes (Lifton et al., 2014). All uncertainties are at the 1 σ level.

Calibration site	St (at g^{-1} yr^{-1})	De (at g^{-1} yr^{-1})	Du (at g^{-1} yr^{-1})	Li (at g^{-1} yr^{-1})	Lm (at g^{-1} yr^{-1})	LSD$_g$ (at g^{-1} yr^{-1})	LSD$_n$ (at g^{-1} yr^{-1})
Grøtlandsura N = 3	3.63 ± 0.15	3.72 ± 0.15	3.69 ± 0.15	3.97 ± 0.16	3.63 ± 0.15	3.46 ± 0.14	3.45 ± 0.14
X^2_R	0.84	0.76	0.77	0.77	0.84	0.78	0.79
Russenes N = 3	4.01 ± 0.20	4.13 ± 0.21	4.09 ± 0.21	4.41 ± 0.22	4.01 ± 0.20	3.83 ± 0.19	3.82 ± 0.19
X^2_R	0.83	0.79	0.79	0.81	0.83	0.82	0.82
Halsnøy N = 8	4.25 ± 0.11	4.36 ± 0.11	4.36 ± 0.11	4.65 ± 0.12	4.25 ± 0.11	4.06 ± 0.10	4.05 ± 0.10
X^2_R	2.96	3.07	3.05	3.00	2.96	3.13	3.11
Oldedalen N = 5	4.16 ± 0.13	4.29 ± 0.14	4.28 ± 0.14	4.56 ± 0.15	4.16 ± 0.13	4.00 ± 0.13	3.99 ± 0.13
X^2_R	2.09	2.04	2.05	2.04	2.09	1.99	2.00
Billingen N = 10	4.04 ± 0.23	4.15 ± 0.24	4.16 ± 0.24	4.44 ± 0.25	4.04 ± 0.23	3.89 ± 0.21	3.88 ± 0.21
X^2_R	1.51	1.52	1.51	1.54	1.51	1.56	1.56
Average A ±1σ SD	**4.02 ± 0.24**	**4.13 ± 0.25**	**4.11 ± 0.26**	**4.41 ± 0.26**	**4.02 ± 0.24**	**3.85 ± 0.24**	**3.84 ± 0.24**
Russenes N = 3	4.01 ± 0.20	4.13 ± 0.21	4.09 ± 0.21	4.41 ± 0.22	4.01 ± 0.20	3.83 ± 0.19	3.82 ± 0.19
X^2_R	0.83	0.79	0.79	0.81	0.83	0.82	0.82
Halsnøy N = 6	4.24 ± 0.11	4.35 ± 0.11	4.34 ± 0.11	4.64 ± 0.12	4.24 ± 0.11	4.05 ± 0.11	4.04 ± 0.11
X^2_R	1.23	1.26	1.25	1.23	1.23	1.30	1.29
Oldedalen N = 4	4.06 ± 0.14	4.19 ± 0.14	4.18 ± 0.14	4.46 ± 0.15	4.06 ± 0.14	3.92 ± 0.13	3.90 ± 0.13
X^2_R	0.61	0.60	0.60	0.60	0.61	0.59	0.59
Billingen bedrock N = 5	4.19 ± 0.20	4.31 ± 0.20	4.31 ± 0.20	4.60 ± 0.22	4.19 ± 0.20	4.04 ± 0.18	4.02 ± 0.18
X^2_R	0.45	0.44	0.44	0.44	0.45	0.44	0.45
Average B[a] ±1σ SD	**4.12 ± 0.11**	**4.24 ± 0.10**	**4.23 ± 0.12**	**4.53 ± 0.11**	**4.13 ± 0.11**	**3.96 ± 0.10**	**3.95 ± 0.10**

[a] The Grøtlandsura production rates are excluded as outliers for average B because they are significantly lower than the other four calibration site production rates. Hence, they are not part of the Scandinavian average reference ^{10}Be production rates.

degradation modelling (Putkonen et al., 2008) and cosmogenic data (Blard et al., 2007) have been used to argue that cobbles are more prone to postglacial shielding than other samples, indicating that the low ^{10}Be concentration of sample S-03-11 and of the other cobble and boulder samples may be due to incomplete exposure. To summarize, although we cannot rule out the possibility of inheritance in the bedrock samples, we interpret the bedrock ^{10}Be concentrations as more reliable than the ^{10}Be concentrations in the boulders and cobbles.

To derive a regional Scandinavian reference ^{10}Be production rate we average the production rates of the various sites. We use an arithmetic average and standard deviation of the site production rates as the regional reference ^{10}Be production rate and uncertainty. This is because the various site production rates are derived by integration over varying lengths of time and because it is difficult to evaluate the robustness of each of the five calibration datasets (cf. Balco et al., 2008; Goehring et al., 2012a). Group A LSD$_n$ reference ^{10}Be production rates range from 3.45 ± 0.14 atoms g^{-1} yr^{-1} (Grøtlandsura) to 4.05 ± 0.10 atoms g^{-1} yr^{-1} (Halsnøy) for the five sites with an average of 3.84 ± 0.24 atoms g^{-1} yr^{-1}. The Grøtlandsura production rate is lower than and has no overlap with the production rates at the other four sites within 1σ uncertainties (Table 3; Figs. 6 and 7) indicating a potential problem with the Grøtlandsura ^{10}Be production rate calibration. The Grøtlandsura production rate also falls outside the respective limits based on Chauvenet's criterion and Peirce's criterion so we consider it an outlier. If the Grøtlandsura production rate is excluded, the four remaining production rates yield an average of 3.94 ± 0.11 atoms g^{-1} yr^{-1} (not shown). To derive production rates based only on tightly clustered ^{10}Be data, group B production rates yield similar average production rates of 3.85 ± 0.24 atoms g^{-1} yr^{-1} for all five calibration sites (not shown) and 3.95 ± 0.10 atoms g^{-1} yr^{-1} if the Grøtlandsura production rate is excluded (Table 3). We favour using the strict average LSD$_n$ reference production rate of 3.95 ± 0.10

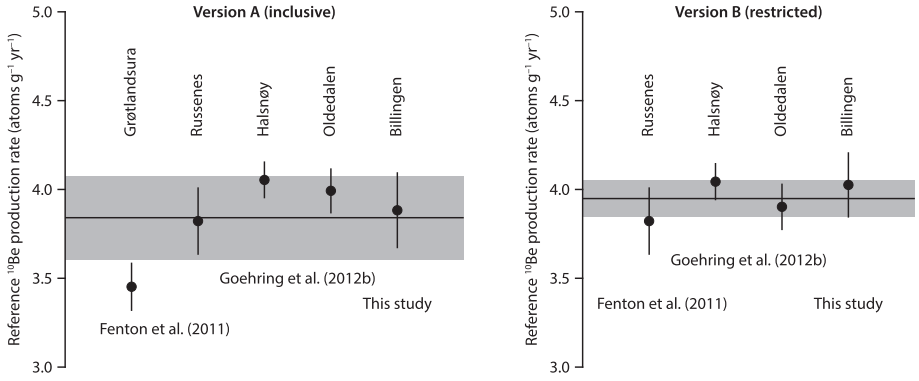

Fig. 7. Local reference ^{10}Be production rates for the LSD$_n$ scaling scheme and arithmetic mean and standard deviation (horizontal black line and grey band). The version A production rates include the full set of samples for all sites except Oldedalen with two outliers rejected. The version B production rates are more restricted requiring $\chi^2_R < 1.5$ and using the Mount Billingen production rate based on the five bedrock samples (Fig. 6). The Grøtlandsura reference production rate of 3.45 ± 0.14 atoms g^{-1} yr^{-1} is excluded as an outlier because it is significantly lower than the other four local reference production rates (Table 3) and because it falls outside the limits of Chauvenet's criterion and Peirce's criterion for outlier rejection. The production rates at Russenes (Fenton et al., 2011), Halsnøy and Oldedalen (Goehring et al., 2012b), and Mount Billingen (this study) for the LSD$_n$ scaling scheme average to a new Scandinavian reference ^{10}Be production rate of 3.95 ± 0.10 atoms g^{-1} yr^{-1}.

atoms g^{-1} yr^{-1} as a regional Scandinavian reference ^{10}Be production rate. This average is based on four local production rates fulfilling the adopted sample cluster criterion ($\chi^2_R < 1.5$) and showing excellent agreement between the various sites (Figs. 6 and 7).

The Scandinavian reference ^{10}Be production rates for the CRONUS scaling schemes are 4–8% lower than the original CRONUS reference production rates (Balco et al., 2008). This is in line with recent ^{10}Be production rate calibrations from various sites around the world (Balco et al., 2009; Putnam et al., 2010; Kaplan et al., 2011; Ballantyne and Stone, 2012; Briner et al., 2012; Blard et al., 2013; Young et al., 2013; Claude et al., 2014; Heyman, 2014; Kelly et al., 2015; Borchers et al., in press) although the Scandinavian production rates are among the highest of the updated production rates. For the CRONUS scaling schemes, the regional Scandinavian production rate (Lm 4.13 ± 0.11 atoms g^{-1} yr^{-1}) is slightly higher than reported production rates for northeastern North America (Balco et al., 2009: Lm 3.85 ± 0.19 atoms g^{-1} yr^{-1}), Greenland (Briner et al., 2012: Lm 3.98 ± 0.24 atoms g^{-1} yr^{-1}), and the general Arctic (Young et al., 2013: Lm 3.96 ± 0.15 atoms g^{-1} yr^{-1}). Compared to the local Norwegian production rates, the Scandinavian average production rate is higher than the production rates from northern Norway (Fenton et al., 2011) but in excellent agreement with the western Norway production rates (Goehring et al., 2012b). Compared to the production rate calibration of Borchers et al. (in press), calibrated using the new CRONUScalc program, the Scandinavian LSD_n production rate of 3.95 ± 0.10 atoms g^{-1} yr^{-1} shows an excellent agreement with their best-fit production rate of 3.92 atoms g^{-1} yr^{-1} (Borchers et al., in press: Sa scaling).

The standard deviation of the four Scandinavian calibration site production rates range from 2.4% to 2.8% of the average production rates for the seven scaling schemes. These uncertainties are lower than the original CRONUS reference production rates (Balco et al., 2008) and recent regional (Balco et al., 2009; Young et al., 2013) and global (Heyman, 2014) recalibration production rates. When calculating ^{10}Be exposure ages of low altitude Scandinavian samples, the regional Scandinavian reference ^{10}Be production rate should yield more accurate and precise exposure ages than those derived from a global production rate.

For the calculation of high elevation ^{10}Be exposure ages, however, some care is advised regarding the production rate uncertainty. The samples used for the Scandinavian production rate calibration were all located at elevations below 150 m a.s.l., implying that the uncertainty of production rate altitudinal scaling (cf. Lifton et al., 2014; Argento et al., 2015a, b) is not captured by the production rate calibration. To calculate exposure ages at high elevations in Scandinavia, a higher production rate uncertainty should be adopted. The global average ^{10}Be production rates of Heyman (2014) range from 5% to 7% and, if we assume that the global uncertainties also capture the altitudinal scaling uncertainty for Scandinavia, then the LSD_n Scandinavian ^{10}Be production rate (with a 6% uncertainty) would become 3.95 ± 0.24 atoms g^{-1} yr^{-1}.

For low elevation samples in Scandinavia, the Scandinavian reference ^{10}Be production rates should yield similar exposure ages for all seven scaling schemes. Borchers et al. (in press) have shown that the two LSD scaling schemes and the CRONUS St and Lm scaling schemes all yield well-clustered reference production rates for various locations and elevations, in contrast to the CRONUS De, Du, and Li scaling schemes which yield more scattered production rates. The LSD scaling schemes, and in particular the nuclide specific LSD_n, are increasingly based on physical principles and should in theory yield more accurate production rates than the St and Lm scaling schemes. However, at present, there is no data confirming this prediction regarding the preference of scaling method (Borchers et al., in press).

6. Conclusions

We present a new reference ^{10}Be production rate calibration dataset with ten samples from the Baltic Ice Lake drainage event at Mount Billingen in southern Sweden at the end of the Younger Dryas and calibrate ^{10}Be production rates for the five CRONUS scaling schemes and the two LSD scaling schemes. Similar to several recent production rate calibration studies, the production rates are lower than the CRONUS global production rates (Balco et al., 2008). Five bedrock samples from surfaces carved by the Baltic Ice Lake drainage event (58.5°N, 13.7°E, 105–120 m a.s.l.) yield a well-clustered reference ^{10}Be production rate of 4.19 ± 0.20 atoms g^{-1} yr^{-1} for the CRONUS Lm scaling and 4.02 ± 0.18 atoms g^{-1} yr^{-1} for the LSD_n scaling. Combining the Mount Billingen production rate with recalibrated ^{10}Be production rates from three sites in Norway yields tightly clustered Scandinavian reference ^{10}Be production rates of 4.13 ± 0.11 atoms g^{-1} yr^{-1} for the CRONUS Lm scaling and 3.95 ± 0.10 atoms g^{-1} yr^{-1} for the LSD_n scaling.

Acknowledgements

We thank P.-H. Blard, V. Rinterknecht, and an anonymous reviewer for valuable reviews that have led to significant improvements. We also thank B. Strömberg for valuable comments on an earlier draft of the manuscript. This work was supported by Swedish Natural Sciences Research Council grant GAA/GU 12034-300 and Swedish Research Council grant G-AA/GU 12034-301 to Stroeven, and National Science Foundation grant 0138486 to Harbor. Sample analyses and support for Caffee were done under the auspices of a PRIME Lab seed grant funded by NSF grant EAR0844151.

Appendix A. Supplementary data

Supplementary data related to this article can be found at http://dx.doi.org/10.1016/j.quageo.2015.06.011.

References

Andrén, T., 2012. Baltic Sea Basin, since the latest deglaciation. In: Bengtsson, L., Herschy, R.W., Fairbridge, R.W. (Eds.), Encyclopedia of Lakes and Reservoirs. Springer Science, pp. 95–102.
Andrén, T., Björck, J., Johnson, S., 1999. Correlation of Swedish glacial varves with the Greenland (GRIP) oxygen isotope record. J. Quat. Sci. 14, 361–371.
Andrén, T., Lindeberg, G., Andrén, E., 2002. Evidence of the final drainage of the Baltic Ice Lake and the brackish phase of the Yoldia Sea in glacial varves from the Baltic Sea. Boreas 31, 226–238.
Applegate, P.J., Urban, N.M., Laabs, B.J.C., Keller, K., Alley, R.B., 2010. Modeling the statistical distributions of cosmogenic exposure dates from moraines. Geosci. Model Dev. 3, 293–307.
Argento, D.C., Stone, J.O., Reedy, R.C., O'Brien, K., 2015a. Physics-based modeling of cosmogenic nuclides part I – radiation transport methods and new insights. Quat. Geochronol. 26, 29–43.
Argento, D.C., Stone, J.O., Reedy, R.C., O'Brien, K., 2015b. Physics-based modeling of cosmogenic nuclides part II – key aspects of *in-situ* cosmogenic nuclide production. Quat. Geochronol. 26, 44–55.
Balco, G., Stone, J.O., Lifton, N.A., Dunai, T.J., 2008. A complete and easily accessible means of calculating surface exposure ages or erosion rates from ^{10}Be and ^{26}Al measurements. Quat. Geochronol. 3, 174–195.
Balco, G., Briner, J., Finkel, R.C., Rayburn, J.A., Ridge, J.C., Schaefer, J.M., 2009. Regional beryllium-10 production rate calibration for late-glacial northeastern North America. Quat. Geochronol. 4, 93–107.
Ballantyne, C.K., Stone, J.O., 2012. Did large ice caps persist on low ground in northwest Scotland during the Lateglacial Interstade? J. Quat. Sci. 27, 297–306.
Berglund, B.E., 1966. Late-Quaternary vegetation in eastern Blekinge, southeastern Sweden. A pollen-analytical study. I. Late-Glacial time. Opera Bot. 12, 1–180.
Berglund, B.E., 1976. The Deglaciation of Southern Sweden. Presentation of a Research Project and a Tentative Radiocarbon Chronology. University of Lund, p. 67. Department of Quaternary Geology Report 10.
Bergsten, K.E., 1943. Isälvsfält kring norra Vättern, vol. VII. Meddelanden från Lunds universitet, pp. 1–245.
Björck, S., 1979. Late Weichselian stratigraphy of Blekinge, SE Sweden, and water level changes in the Baltic Ice Lake. Department of Quaternary Geology.

University of Lund, Lund, p. 248.
Björck, S., 1981. A stratigraphic study of Late Weichselian deglaciation shore displacement and vegetation history in south-eastern Sweden. Fossils Strata 14, 1–93.
Björck, S., 1995. A review of the history of the Baltic Sea, 13.0-8.0 ka BP. Quat. Int. 27, 19–40.
Björck, S., 2008. The late quaternary development of the Baltic Sea. In: BACC Author Team (Ed.), Assessment of Climate Change for the Baltic Sea Basin. Springer-Verlag Berlin Heidelberg, pp. 398–407.
Björck, S., Digerfeldt, G., 1984. Climatic changes at pleistocene/holocene boundary in the middle Swedish endmoraine zone, mainly inferred from stratigraphic indications. In: Mörner, N.-A., Karlén, W. (Eds.), Climatic Changes on a Yearly to Millennial Basis: Geological, Historical and Instrumental Records. D. Reidel Publishing Company, Dordrecht/Boston/Lancaster, pp. 37–56.
Björck, S., Digerfeldt, G., 1986. Late Weichselian-early holocene shore displacement west of Mt. Billingen, within the middle Swedish end moraine zone. Boreas 15, 1–18.
Björck, S., Digerfeldt, G., 1989. Lake Mullsjön — a key site for understanding the final stage of the Baltic Ice Lake east of Mt. Billingen. Boreas 18, 209–219.
Björck, S., Wohlfarth, B., Possnert, G., 1995. ^{14}C AMS measurements from the Late Weichselian part of the Swedish Time Scale. Quat. Int. 27, 11–18.
Björck, S., Kromer, B., Johnsen, S., Bennike, O., Hammarlund, D., Lemdahl, G., Possnert, G., Rasmussen, T.L., Wohlfarth, B., Hammer, C.U., Spurk, M., 1996. Synchronized terrestrial-atmospheric deglacial records around the North Atlantic. Science 274, 1155–1160.
Blard, P.-H., Lavé, J., Pik, R., Wagnon, P., Bourlès, D., 2007. Persistence of full glacial conditions in the central Pacific until 15,000 years ago. Nature 449, 591–596.
Blard, P.-H., Braucher, R., Lavé, J., Bourlès, D., 2013. Cosmogenic ^{10}Be production rate calibrated against ^{3}He in the high Tropical Andes (3800–4900 m, 20–22° S). Earth Planet. Sci. Lett. 382, 140–149.
Bodén, P., Fairbanks, R.G., Wright, J.D., Burckle, L.H., 1997. High-resolution isotope records from southwest Sweden: the drainage of the Baltic Ice Lake and Younger Dryas ice margin oscillations. Paleoceanography 12, 39–49.
Borchers, B., Marrero, S., Balco, G., Caffee, M., Goehring, B., Lifton, N., Nishiizumi, K., Phillips, F., Schaefer, J., Stone, J., 2015. Geological calibration of spallation production rates in the CRONUS-Earth project. Quat. Geochronol. 1–12 (in press).
Boulton, G.S., Dongelmans, P., Punkari, M., Broadgate, M., 2001. Palaeoglaciology of an ice sheet through a glacial cycle: the European ice sheet through the Weichselian. Quat. Sci. Rev. 20, 591–625.
Briner, J.P., Young, N.E., Goehring, B.M., Schaefer, J.M., 2012. Constraining holocene ^{10}Be production rates in Greenland. J. Quat. Sci. 27, 2–6.
Bronk Ramsey, C., 2009. Bayesian analysis of radiocarbon dates. Radiocarbon 51, 337–360.
Brown, E.T., Edmond, J.M., Raisbeck, G.M., Yiou, F., Kurz, M.D., Brook, E.J., 1991. Examination of surface exposure ages of Antarctic moraines using *in situ* produced ^{10}Be and ^{26}Al. Geochim. Cosmochim. Acta 55, 2269–2283.
Caldenius, C., 1944. Baltiska issjöns sänkning till Västerhavet. Geol. Fören. Stockh. Förh. 66, 366–382.
Child, D., Elliott, G., Mifsud, C., Smith, A.M., Fink, D., 2000. Sample processing for earth science studies at ANTARES. Nucl. Instrum. Methods Phys. Res. Sect. B Beam Interact. Mater. Atoms 172, 856–860.
Chmeleff, J., von Blanckenburg, F., Kossert, K., Jakob, D., 2010. Determination of the 10Be half-life by multicollector ICP-MS and liquid scintillation counting. Nucl. Instrum. Methods Phys. Res. B Beam Interact. Mater. Atoms 268, 192–199.
Claude, A., Ivy-Ochs, S., Kober, F., Antognini, M., Salcher, B., Kubik, P.W., 2014. The Chironico landslide (Valle Leventina, southern Swiss Alps): age and evolution. Swiss J. Geosci. 107, 273–291.
Cleve-Euler, A., 1946. Om den sista landisens bortsmältning från Södra Sverige, den s.k. Baltiska issjön, tappningarna vid Billingen och Degerfors samt Vätterns historia — Jämte ett tillägg om norska isgränser. Stockholm.
De Geer, G., 1884. Om möjligheten af att införa en kronologi för Istiden. Geol. Fören. Stockh. Förh. 7, 3.
De Geer, G., 1896. Skandinaviens geografiska utveckling efter istiden, 161. Sveriges Geologiska Undersökning, Ser C, pp. 1–160.
De Geer, G., 1912. In: . A Geochronology of the Last 12 000 Years, Proceedings of the 11th International Geological Congress 1910, Stockholm, pp. 243–253.
De Geer, G., 1940. Geochronologia Sueccia principles. K. Sven. Vetensk. Handl. III 18 (6), 367.
Desilets, D., Zreda, M., 2003. Spatial and temporal distribution of secondary cosmic-ray nucleon intensities and applications to in situ cosmogenic dating. Earth Planet. Sci. Lett. 206, 21–42.
Desilets, D., Zreda, M., Prabu, T., 2006. Extended scaling factors for in situ cosmogenic nuclides: new measurements at low latitude. Earth Planet. Sci. Lett. 246, 265–276.
Donner, J.J., 1969. Land/sea level changes in southern Finland during the formation of the Salpausselkä endmoraines. Bull. Geol. Soc. Finl. 41, 135–150.
Donner, J.J., 1978. The dating of the levels of the Baltic Ice Lake and the Salpausselkä moraines in South Finland. Societas Scientiarum Fennica. Comment. Phys. Math. 48, 11–38.
Dunai, T.J., 2000. Scaling factors for production rates of in situ produced cosmogenic nuclides: a critical reevaluation. Earth Planet. Sci. Lett. 176, 157–169.
Dunai, T.J., 2001. Influence of secular variation of the geomagnetic field on production rates of in situ produced cosmogenic nuclides. Earth Planet. Sci. Lett. 193, 197–212.
Erlenkeuser, H., 1985. Stable isotopes in benthic foraminifers of Skagerrak core GIK 15530-4: high resolution record of the Younger Dryas and the Holocene. Nor. Geol. Tidsskr. 65, 49–57.
Fenton, C.R., Hermanns, R.L., Blikra, L.H., Kubik, P.W., Bryant, C., Niedermann, S., Meixner, A., Goethals, M.M., 2011. Regional ^{10}Be production rate calibration for the past 12 ka deduced from the radiocarbon-dated Grøtlandsura and Russenes rock avalanches at 69 °N. Nor. Quat. Geochronol. 6, 437–452.
Gavelin, A., 1926. Comments on a lecture. Geol. Fören. Stockh. Förh. 48, 292–294.
Goehring, B.M., Lohne, Ø.S., Mangerud, J., Svendsen, J.I., Gyllencreutz, R., Schaefer, J., Finkel, R., 2012a. Erratum: late glacial and holocene ^{10}Be production rates for western Norway. J. Quat. Sci. 27, 544.
Goehring, B.M., Lohne, Ø.S., Mangerud, J., Svendsen, J.I., Gyllencreutz, R., Schaefer, J., Finkel, R., 2012b. Late glacial and holocene ^{10}Be production rates for western Norway. J. Quat. Sci. 27, 89–96.
Gosse, J.C., Phillips, F.M., 2001. Terrestrial in situ cosmogenic nuclides: theory and application. Quat. Sci. Rev. 20, 1475–1560.
Heyman, J., 2014. Paleoglaciation of the Tibetan Plateau and surrounding mountains based on exposure ages and ELA depression estimates. Quat. Sci. Rev. 91, 30–41.
Heyman, J., Stroeven, A.P., Harbor, J.M., Caffee, M.W., 2011. Too young or too old: evaluating cosmogenic exposure dating based on an analysis of compiled boulder exposure ages. Earth Planet. Sci. Lett. 302, 71–80.
Hyttinen, O., Eskola, K.O., Kaakinen, A., Salonen, V.-P., 2014. First direct age determination for the Baltic Ice Lake/Yoldia Sea transition in Finland. GFF 136, 398–405.
Jakobsson, M., Björck, S., Alm, G., Andrén, T., Lindeberg, G., Svensson, N.-O., 2007. Reconstructing the Younger Dryas ice dammed lake in the Baltic Basin: Bathymetry, area and volume. Glob. Planet. Change 57, 355–370.
Johansson, S., 1926. Baltiska issjöns tappning. Geol. Fören. Stockh. Förh. 48, 186–263.
Johansson, S., 1937. Senglaciala och interglacial avlagringar vid ändmoranstråket i Västergötland. Geol. Fören. Stockh. Förh. 59, 379–454.
Johnson, M.D., Ståhl, Y., Larsson, O., Seger, S., 2010. New exposures of Baltic Ice Lake drainage sediments, Götene, Sweden. GFF 132, 1–12.
Johnson, M.D., Benediktsson, I.Ö., Björklund, L., 2013a. The Ledsjö end moraine – a subaquatic push moraine composed of glaciomarine clay in central Sweden. Proc. Geol. Assoc. 124, 738–752.
Johnson, M.D., Kylander, M.E., Casserstedt, L., Wiborgh, H., Bjorck, S., 2013b. Varved glaciomarine clay in central Sweden before and after the Baltic Ice Lake drainage: a further clue to the drainage events at Mt Billingen. GFF 135, 293–307.
Kaplan, M.R., Strelin, J.A., Schaefer, J.M., Denton, G.H., Finkel, R.C., Schwartz, R., Putnam, A.E., Vandergoes, M.J., Goehring, B.M., Travis, S.G., 2011. In-situ cosmogenic 10Be production rate at Lago Argentino, Patagonia: implications for late-glacial climate chronology. Earth Planet. Sci. Lett. 309, 21–32.
Kelly, M.A., Lowell, T.V., Applegate, P.J., Phillips, F.M., Schaefer, J.M., Smith, C.A., Kim, H., Leonard, K.C., Hudson, A.M., 2015. A locally calibrated, late glacial ^{10}Be production rate from a low-latitude, high-altitude site in the Peruvian Andes. Quat. Geochronol. 26, 70–85.
Klein, J., Giegengack, R., Middleton, R., Sharma, P., Underwood, J.R., 1986. Revealing histories of exposure using in situ produced 26Al and 10Be in Libyan desert glass. Radiocarbon 28, 547–555.
Kleman, J., Hättestrand, C., Borgström, I., Stroeven, A., 1997. Fennoscandian paleoglaciology reconstructed using a glacial geological inversion model. J. Glaciol. 43, 283–299.
Kohl, C.P., Nishiizumi, K., 1992. Chemical isolation of quartz for measurement of in situ-produced cosmogenic nuclides. Geochim. Cosmochim. Acta 56, 3586–3587.
Korschinek, G., Bergmaier, A., Faestermann, T., Gerstmann, U.C., Knie, K., Rugel, G., Wallner, A., Dillmann, I., Dollinger, G., Liese von Gostomski, C., Kossert, K., Maiti, M., Poutivtsev, M., Remmert, A., 2010. A new value for the half-life of ^{10}Be by heavy-ion elastic recoil detection and liquid scintillation counting. Nucl. Instrum. Methods Phys. Res. B Beam Interact. Mater. Atoms 268, 187–191.
Kurz, M.D., 1986a. Cosmogenic helium in a terrestrial igneous rock. Nature 320, 435–439.
Kurz, M.D., 1986b. *In situ* production of terrestrial cosmogenic helium and some applications to geochronology. Geochim. Cosmochim. Acta 50, 2855–2862.
Lal, D., 1991. Cosmic ray labeling of erosion surfaces: *in situ* nuclide production rates and erosion models. Earth Planet. Sci. Lett. 104, 424–439.
Lambeck, K., 1999. Shoreline displacements in southern-central Sweden and the evolution of the Baltic Sea since the last maximum glaciation. J. Geol. Soc. Lond. 156, 465–486.
Lifton, N.A., Bieber, J.W., Clem, J.M., Duldig, M.L., Evenson, P., Humble, J.E., Pyle, R., 2005. Addressing solar modulation and long-term uncertainties in scaling secondary cosmic rays for in situ cosmogenic nuclide applications. Earth Planet. Sci. Lett. 239, 140–161.
Lifton, N., Smart, D.F., Shea, M.A., 2008. Scaling time-integrated in situ cosmogenic nuclide production rates using a continuous geomagnetic model. Earth Planet. Sci. Lett. 268, 190–201.
Lifton, N., Sato, T., Dunai, T.J., 2014. Scaling *in situ* cosmogenic nuclide production rates using analytical approximations to atmospheric cosmic-ray fluxes. Earth Planet. Sci. Lett. 386, 149–160.
Lindeberg, G., 2002. The Swedish Varved Clays Revisited: Spectral- and Image Analysis of Different Types of Varve Series from the Baltic Basin. Department of Physical Geography and Quaternary Geology. Stockholm University, Stockholm. Thesis in Quaternary Geology, No. 1.
Lohne, Ø.S., Mangerud, J., Svendsen, J.I., 2012. Timing of the Younger Dryas glacial

maximum in western Norway. J. Quat. Sci. 27, 81–88.
Lundqvist, G., 1921. Den baltiska issjöns tappning och strandlinjerna vid Billingens nordspets. Geol. Fören. Stockh. Förh. 43, 381–385.
Lundqvist, G., 1931. Jordlagren. In: Lundqvist, G., Högbom, A., Westergårdh, A.H. (Eds.), Beskrivning till geologiska kartbladet Lugnås. Sveriges Geologiska Undersökning, p. 185. Aa 172.
Lundqvist, J., Wohlfarth, B., 2001. Timing and east-west correlation of south Swedish ice marginal lines during the Late Weichselian. Quat. Sci. Rev. 20, 1127–1148.
Masarik, J., Frank, M., Schäfer, J.M., Wieler, R., 2001. Correction of in situ cosmogenic nuclide production rates for geomagnetic field intensity variations during the past 800,000 years. Geochim. Cosmochim. Acta 65, 2995–3003.
Mörner, N.-A., 1969. The late quaternary history of the Kattegatt Sea and the Swedish west coast; Deglaciation, shorelevel displacement, chronology, isostasy and eustasy. Sver. Geol. Unders. C640, 487.
Mörner, N.-A., 1979. The fennoscandian uplift and late cenozoic geodynamics: geological evidence. GeoJournal 3.3, 287–318.
Munthe, H., 1910. Studies in the late-quaternary history of southern Sweden. Geol. Fören. Stockh. Förh. 32, 1197–1293.
Munthe, H., 1912. The exploration of Valle Härad, Sweden. Z. Gletscherkd. Glazialgeol. 6, 347–348.
Munthe, H., 1928. Drag ur den senglaciala utvecklingen av Billingen-Falbygden med omnejd. Geol. Fören. Stockh. Förh. 50, 233–286.
Munthe, H., 1940. Om Nordens, främst Baltikums, senkvartära utveckling och stenåldersbebyggelse. K. Sven. Vetenskap. Handl. Ser. III 19, 1–242.
Munthe, H., Westergård, A.H., Lundqvist, G., 1928. Beskrivning till kartbladet Skövde. Sver. Geol. Unders. Ser. Aa 121, 1–182.
Muscheler, R., Kromer, B., Björck, S., Svensson, A., Friedrich, M., Kaiser, K.F., Southon, J., 2008. Tree rings and ice cores reveal ^{14}C calibration uncertainties during the Younger Dryas. Nat. Geosci. 1, 263–267.
Nishiizumi, K., Lal, D., Klein, J., Middleton, R., Arnold, J.R., 1986. Production of ^{10}Be and ^{26}Al by cosmic rays in terrestrial quartz *in situ* and implications for erosion rates. Nature 319, 134–136.
Nishiizumi, K., Winterer, E.L., Kohl, C.P., Klein, J., Middleton, R., Lal, D., Arnold, J.R., 1989. Cosmic ray production rates of ^{10}Be and ^{26}Al in quartz from glacially polished rocks. J. Geophys. Res. 94, 17907–17915.
Nishiizumi, K., Imamura, M., Caffee, M.W., Southon, J.R., Finkel, R.C., McAninch, J., 2007. Absolute calibration of ^{10}Be AMS standards. Nucl. Instrum. Methods Phys. Res. Sect. B Beam Interact. Mater. Atoms 258, 403–413.
Olausson, E., 1982. Stable isotopes. Sver. Geol. Unders. C794, 82–92.
Påsse, T., 1987. Shore displacement during the Late Weichselian and holocene in the Sandsjöbacka area, SW Sweden. Geol. Fören. Stockh. Förh. 109, 197–201.
Phillips, F.M., Leavy, B.D., Jannik, N.O., Elmore, D., Kubik, P.W., 1986. The accumulation of cosmogenic chlorine-36 in rocks: a method for surface exposure dating. Science 231, 41–43.
Pizarro Rajala, E., 2012. En sedimentologisk analys av Timmersdalaryggen i Västergötland, Sverige. Göteborg University. Bachelor of Science thesis.
Putkonen, J., Connolly, J., Orloff, T., 2008. Landscape evolution degrades the geologic signature of past glaciations. Geomorphology 97, 208–217.
Putnam, A.E., Schaefer, J.M., Barrell, D.J.A., Vandergoes, M., Denton, G.H., Kaplan, M.R., Finkel, R.C., Schwartz, R., Goehring, B.M., Kelley, S.E., 2010. In situ cosmogenic ^{10}Be production-rate calibration from the Southern Alps, New Zealand. Quat. Geochronol. 5, 392–409.
Rasmussen, S.O., Bigler, M., Blockley, S.P., Blunier, T., Buchardt, S.L., Clausen, H.B., Cvijanovic, I., Dahl-Jensen, D., Johnsen, S.J., Fischer, H., Gkinis, V., Guillevic, M., Hoek, W.Z., Lowe, J.J., Pedro, J.B., Popp, T., Seierstad, I.K., Steffensen, J.P., Svensson, A.M., Vallelonga, P., Vinther, B.M., Walker, M.J.C., Wheatley, J.J., Winstrup, M., 2014. A stratigraphic framework for abrupt climatic changes during the last glacial period based on three synchronized Greenland ice-core records: refining and extending the INTIMATE event stratigraphy. Quat. Sci. Rev. 106, 14–28.
Reimer, P.J., Bard, E., Bayliss, A., Beck, J.W., Blackwell, P.G., Ramsey, C.B., Buck, C.E., Cheng, H., Edwards, R.L., Friedrich, M., Grootes, P.M., Guilderson, T.P., Haflidason, H., Hajdas, I., Hatté, C., Heaton, T.J., Hoffmann, D.L., Hogg, A.G., Hughen, K.A., Kaiser, K.F., Kromer, B., Manning, S.W., Niu, M., Reimer, R.W., Richards, D.A., Scott, E.M., Southon, J.R., Staff, R.A., Turney, C.S.M., van der Plicht, J., 2013. Intcal13 and Marine13 radiocarbon age calibration curves 0–50,000 years cal BP. Radiocarbon 55, 1869–1887.
Sato, T., Yasuda, H., Niita, K., Endo, A., Sihver, L., 2008. Development of PARMA: PHITS-based analytical radiation model in the atmosphere. Radiat. Res. 170, 244–259.
Sauramo, M., 1934. Zur spätquartären Geschichte der Ostsee. Bull. Comm. Géol. Finl. 104, 28–87.
Sauramo, M., 1937. Das System der spätglazialen Strandlinien im südlichen Finnland. Societas Scientiarum Fennica. Comment. Phys. Math. 9, 23.
Sauramo, M., 1958. Die Geschichte der Ostsee. Ann. Acad. Sci. Fenn. A III 51, 1–522.
Staiger, J., Gosse, J., Toracinta, R., Oglesby, B., Fastook, J., Johnson, J.V., 2007. Atmospheric scaling of cosmogenic nuclide production: climate effect. J. Geophys. Res. Solid Earth 112, B02205.
Stone, J.O., 2000. Air pressure and cosmogenic isotope production. J. Geophys. Res. 105, 23753–23759.
Stroeven, A.P., Hättestrand, C., Kleman, J., Heyman, J., Fabel, D., Fredin, O., Goodfellow, B.W., Harbor, J.M., Jansen, J.D., Olsen, L., Caffee, M.W., Fink, D., Lundqvist, J., Rosqvist, G.C., Strömberg, B., Jansson, K.N., 2015. Deglaciation of Fennoscandia. Quaternary Science Reviews (in review).
Stroeven, A.P., Fabel, D., Harbor, J.M., Fink, D., Caffee, M.W., Dahlgren, T., 2011. Importance of sampling across an assemblage of glacial landforms for interpreting cosmogenic ages of deglaciation. Quat. Res. 76, 148–156.
Strömberg, B., 1974. Billingenområdet vid slutet av den senaste istiden. Skaraborgsnatur 11, 2–16.
Strömberg, B., 1977a. Deglaciationen vid Billingen och Baltiska Issjöns tappning. Geol. Fören. Stockh. Förh. 99, 92–95.
Strömberg, B., 1977b. Einige Bemerkungen zum Rückzug des Inlandeises am Billingen (Västergötland, Schweden) und dem Ausbruch des Baltischen Eisstausees. Zeitschrift für Geomorphologie N.F. Supplementband 27, 89–111.
Strömberg, B., 1985. New varve measurements in Västergötland, Sweden. Boreas 14, 111–115.
Strömberg, B., 1992. The final stage of the Baltic Ice Lake. Sver. Geol. Unders. Ca 81, 347–353.
Strömberg, B., 1994. Younger Dryas deglaciation at Mt. Billingen, and clay varve dating of the Younger Dryas/preboreal transition. Boreas 23, 177–193.
Svedhage, K., 1985. Shore Displacement during Late Weichselian and Early Holocene in the Risveden Area, SW Sweden, Geologiska institutionen. Chalmers Tekniska Hogskola/Göteborgs universitet, p. 111. PhD Thesis.
Svensson, N.-O., 1989. Late Weichselian and Early Holocene Shore Displacement in the Central Baltic, Based on Stratigraphical and Morphological Records from Eastern Småland and Gotland, Sweden. Lund University, p. 195. PhD Thesis, Lundqua thesis 25.
Svensson, N.-O., 1991. Late Weichselian and early holocene shore displacement in the central Baltic Sea. Quat. Int. 9, 7–26.
Tikkanen, M., Oksanen, J., 2002. Late Weichselian and holocene shore displacement history of the Baltic Sea in Finland. Fennia 180, 9–20.
Walker, M., Johnsen, S., Rasmussen, S.O., Popp, T., Steffensen, J.P., Gibbard, P., Hoek, W., Lowe, J., Andrews, J., Bjorck, S., Cwynar, L.C., Hughen, K., Kershaw, P., Kromer, B., Litt, T., Lowe, D.J., Nakagawa, T., Newnham, R., Schwander, J., 2009. Formal definition and dating of the GSSP (Global Stratotype Section and Point) for the base of the holocene using the Greenland NGRIP ice core, and selected auxiliary records. J. Quat. Sci. 24, 3–17.
Westergård, A.H., 1926. Kvartärsystemet. In: Westergård, A.H., Johansson, H.E., Willén, N. (Eds.), Beskrivning till kartbladet Karlsborg. Sveriges Geologiska Undersökning, Aa, vol. 162, pp. 1–96.
Young, N.E., Schaefer, J.M., Briner, J.P., Goehring, B.M., 2013. A ^{10}Be production-rate calibration for the Arctic. J. Quat. Sci. 28, 515–526.